JOURNAL OF SPACECRAFT AND ROCKETS
Vol. 33, No. 3, May–June 1996

Numerical Investigation of Laminar-Turbulent Transition on Re-Entry Capsules

E. Laurien*
Technical University of Braunschweig, D-38106 Braunschweig, Germany

Transition from laminar to turbulent flow in the boundary layer of blunt cones under re-entry conditions from space is investigated using the tool of numerical simulation. Two- and three-dimensional disturbances appear to be linearly stable (using classical linear stability theory) in a wide range of wave numbers under conditions for which wind-tunnel experiments exhibit turbulence. Therefore, linear mechanisms cannot describe transition, and the e^N method cannot be used for transition prediction. It is shown that a nonlinear instability with respect to finite amplitude local disturbances exists. This instability leads to the formation of turbulent spots. Using a generic trajectory of a re-entry capsule at an altitude of 75 km, where the boundary layer is laminar, our investigation does not exhibit any instability as expected. At 20 km, where the boundary layer is turbulent, nonlinear instability is found. Therefore, our theory provides suitable ground for the development of new nonlinear transition criteria.

Nomenclature

A	= initial disturbance amplitude parameter
c	= complex phase velocity
D	= base diameter of conical body, m
f_1, f_2, f_3, f_4	= functions used for smoothing
j	= index of streamwise station
k_1	= index of streamwise Fourier modes
k_2	= index of transverse Fourier modes
L_1, L_2	= lengths of numerical simulation domain
M	= Mach number
q	= heat flux, J/m^{2}s
R	= nose radius, m
Re	= Reynolds number
s	= coordinate along the body contour, m
T	= temperature, K
u	= wall-parallel velocity component, m/s
u_1, u_2, u_3	= velocity components in the numerical simulation domain
x	= coordinate along the body axis, m
x_1, x_2, x_3	= coordinates of the numerical simulation domain
y	= wall normal coordinate, m
α	= streamwise wave number
β	= transverse wave number
δ	= boundary layer thickness, m
ε	= radiation coefficient
λ_1, λ_2	= coefficients for smoothing
μ	= coefficient for smoothing
ρ	= density, kg/m^3

Subscripts

e	= boundary-layer edge
TS	= Tollmien–Schlichting wave
w	= wall
δ	= based on boundary-layer thickness
∞	= freestream

Introduction

TRANSITION from laminar to turbulent boundary layers begins with an amplification of various types of disturbances (two dimensional, three dimensional, small, large) that are present in a flow. Transition mechanisms on subsonic and transonic airplane wings have been investigated in detail and can be modeled using the e^N method; e.g., Ref. 1. On those wings, transition begins with small amplitude waves generated by either the linear Tollmien–Schlichting or crossflow instability. Attachment-line instability may occur as well. At supersonic Mach numbers three-dimensional disturbances and second-mode disturbances become additionally unstable.

In the present paper, we consider transition in the boundary layer of re-entry capsules. In contrast to the preceding situations, the mechanisms of transition are unknown. Our aim is to develop more general transition criteria for re-entry flows based on theory. Transition criteria, e.g., Ref. 2, are purely empirical rather than based on stability theory. We use both linear stability theory and nonlinear simulation methods to understand transition mechanism.

A typical model body geometry is shown in Fig. 1. It is a 9-deg cone with a spherical nose. Wind-tunnel experiments at $M_\infty = 5$ (cold hypersonic flow) with the aim to investigate the transition location have been performed by Widhopf and Hall,[3] using a model with a nose radius $R = 6.1$ cm. The measured wall heat flux data are

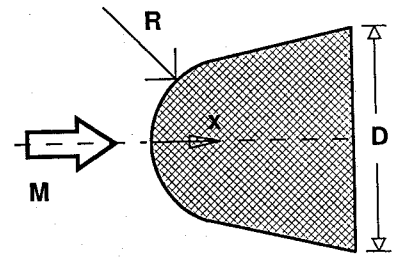

Fig. 1 Considered blunt body geometry.

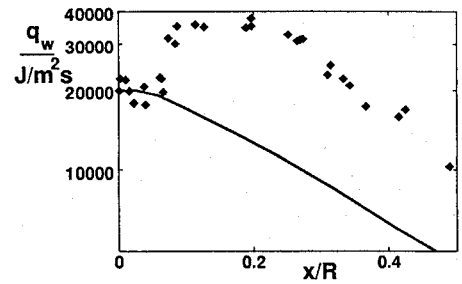

Fig. 2 Surface heat flux comparison: ♦, Ref. 3 and —, laminar Navier–Stokes solution.

Presented as Paper 95-0775 at the AIAA 33rd Aerospace Sciences Meeting and Exhibit, Reno, NV, Jan. 9–12, 1995; received Feb. 3, 1995; revision received Aug. 22, 1995; accepted for publication Aug. 22, 1995.

*Scientist, Institute for Fluid Mechanics, Bienroder Weg 3. Member AIAA.

depicted in Fig. 2 together with a laminar Navier–Stokes solution using our finite element method (perfect gas). The sharp rise of the measured heat flux because of laminar-turbulent transition by more than a factor of two becomes evident. Transition takes place at a location on the spherical nose rather than on the conical portion of the body.

Hypersonic boundary-layer transition related to re-entry flows has been investigated using long slender cones.[4–6] In contrast to those studies, the geometry we consider is a very short cone with large bluntness. The boundary layer at the location of transition is subsonic or transonic rather than hypersonic.

Numerical Simulation of Re-Entry Flows

A generic trajectory of a re-entry capsule[7] is assumed. For our investigations we choose two points on this trajectory: 1) at 75-km altitude with a Mach number $M_\infty = 27$ and a Reynolds number $Re_D = 21{,}000$ and 2) at 20-km altitude at $M_\infty = 5$, $Re_D = 9 \times 10^6$. In case 1 the geometry is slightly modified as suggested in Ref. 7 to an axisymmetric nose with elliptical cross section (half axes 0,458 m and 0,285 m, cone angle 11 deg). Case 2 corresponds in geometry and flow parameters to the experiments of Ref. 3, where turbulent flow is expected. The empirical criterion of Ref. 2 predicts laminar flow for case 1 and turbulent flow for case 2.

For our computations of the laminar base flows, which are used for stability investigations, the finite element code of Laurien et al.[8] is used. This code was developed to simulate high-temperature chemically reacting re-entry flows under a wide range of inflow conditions. It is based on the Taylor–Galerkin finite element method by Löhner et al.[9] and implemented on various supercomputers.[10] The high-temperature chemistry model of Park was implemented.[11,12]

During the computations a relatively coarse initial grid was successively refined until deviations of all flow quantities between the two finest grids were smaller than approximately 1% of their values. For each grid, numerical iteration (time steps) were performed as long as the residual was reduced at least by a factor of two within 50% of the total number of time steps. To ensure convergence, more than 10,000 time steps were needed for case 1. A typical locally refined grid including the boundary layer and the bow shock is shown in Fig. 3.

Computations were performed under the following assumptions. For case 1, nonequilibrium chemically reacting air with thermal equilibrium and noncatalytic wall is assumed. Equilibrium between the surface heat flux and a radiation cooling ($\varepsilon = 0.85$) is assumed so that the surface temperature is a result of the computation (approximately 1400 K at the nose). For case 2, perfect gas with isothermal wall ($T_W/T_\infty = 1.56$) is assumed.

In a postprocessing step of the base flow computations, the boundary-layer thickness δ was determined as the wall distance where the wall-parallel velocity component is reduced because of the no-slip condition at the wall. The determination of δ was done subjectively rather than automatically (an automatical procedure, e.g., based on velocity gradients, would not be appropriate, because the velocity outside the boundary layer is not constant). Additionally, it was checked that the corresponding thermal boundary layer is thinner than the velocity boundary layer.

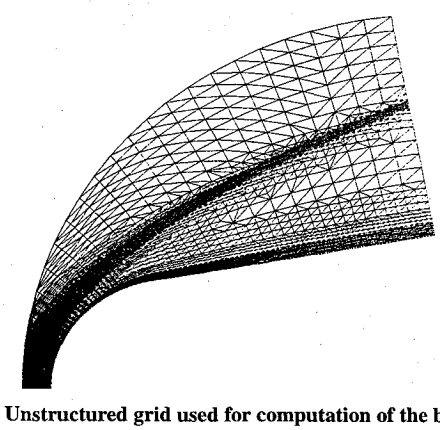

Fig. 3 Unstructured grid used for computation of the base flow.

Table 1 Stations s/D along the body surface of case 1 and corresponding boundary-layer thickness δ/D

j	1	2	3	4	5
s/D	0	0.37	0.74	1.12	1.49
δ_j/D	0.026	0.040	0.054	0.060	0.063

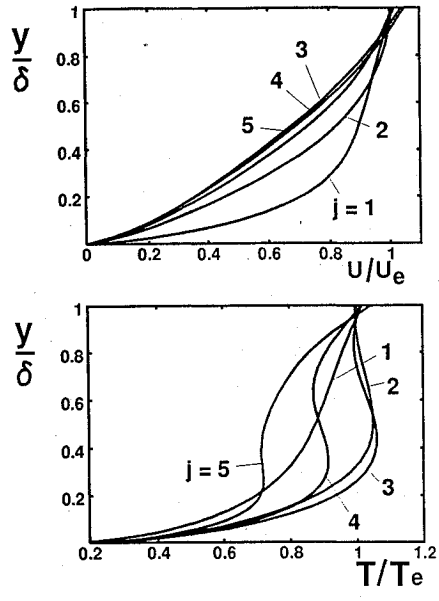

Fig. 4 Base flow velocity and temperature within the boundary layer at stations j of Table 1, case 1.

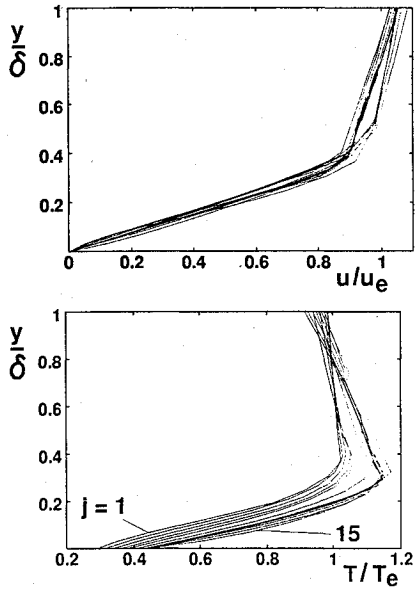

Fig. 5 Base flow velocity and temperature within the boundary layer at stations j of Table 2, case 2.

For case 1, the boundary-layer thickness δ/D (where D is the base diameter at $x = 1.39$ m) at five stations s/D (where s is the coordinate along the body contour starting at the nose) is determined as shown in Table 1. The corresponding profiles of the wall-parallel velocity u/u_e, temperature T/T_e, and density ρ/ρ_e are shown in Fig. 4. Here and in the following, the wall normal coordinate y is normalized with the local boundary-layer thickness δ, and the flow quantities are normalized by their respective values at the boundary-layer edge (index e).

For case 2, the boundary-layer thickness is determined at 15 stations s/R as shown in Table 2. In Fig. 5 velocity and temperature profiles at these stations are shown. The temperature profiles of the figure correspond from left to right (at $y/\delta = 0$) to those stations. All velocity profiles (not labeled) are almost identical in the

Table 2 Stations s/R along the body surface of case 2 and corresponding boundary-layer thickness δ/R

j	1	2	3	4	5	6	7	8	9	10	11	12	13	14	15
s/R	0	0.23	0.46	0.68	0.91	1.14	1.37	1.60	1.82	2.05	2.28	2.50	2.73	2.96	3.19
δ_j/R	0.014	0.016	0.019	0.023	0.030	0.040	0.057	0.081	0.105	0.12	0.13	0.14	0.14	0.15	0.15

normalized coordinates. The flow exhibits the character of an accelerated boundary layer along a cooled wall.

Linear Stability Results

Linear stability theory based on compressible three-dimensional perturbation equations is applied. Because stability results are known to be sensitive with respect to discontinuities of the spatial derivatives of the base profiles, smoothing becomes necessary. We use curve fits of our profiles, e.g., for the velocity,

$$u/u_e = (1-\mu)f_1 + \mu f_3 + \lambda_1 f_2 + \lambda_2 f_4 \tag{1}$$

where f_1 and f_2 are the Pohlhausen functions

$$f_1 = 2(y/\delta) - 2(y/\delta)^3 + (y/\delta)^4 \tag{2}$$

$$f_2 = \tfrac{1}{6}[(y/\delta) - 3(y/\delta)^2 + 3(y/\delta)^3 - (y/\delta)^4] \tag{3}$$

and f_3 and f_4 are additional functions defined as

$$f_3 = 8.33(y/\delta) - 30.33(y/\delta)^2 + 63(y/\delta)^3 - 81.67(y/\delta)^4 + 67.67(y/\delta)^5 - 35(y/\delta)^6 + 10.33(y/\delta)^7 - 1.33(y/\delta)^8 \tag{4}$$

$$f_4 = 0.167(y/\delta) - 1.167(y/\delta)^2 + 3.5(y/\delta)^3 - 5.833(y/\delta)^4 + 5.833(y/\delta)^5 - 3.5(y/\delta)^6 + 1.167(y/\delta)^7 - 0.167(y/\delta)^8 \tag{5}$$

These functions are shown in Fig. 6, together with an example curve fit. The functions f_3 and f_4 were added to the original Pohlhausen family to control the near-wall behavior of the approximation. Their coefficients were determined such that, at the wall, their first derivatives are 1/6 for f_3 and 50/6 for f_4, and some higher derivatives are zero.

For each case, the profile at one particular station (see Tables 1 and 2) located in the outer region of the blunt nose was chosen: for case 1, profile 2, at $s/D = 0.37$ with the velocity approximated by $\mu = 0.86$, $\lambda_1 = -8$, and $\lambda_2 = 10$ (Reynolds number based on boundary-layer thickness and velocity at the boundary-layer edge is $Re_\delta = 171$); for case 2, profile 7, at $s/R = 1.37$ with $\mu = 0.85$, $\lambda_1 = -0.5$, and $\lambda_2 = -25$ ($Re_\delta = 3000$).

It appears that both profiles of cases 1 and 2 are linearly stable in a wide range of wave numbers in streamwise and spanwise directions, α and β. Damping rates imag$\{c_{TS}\}$, with c_{TS} being the complex phase velocity of the least damped (Tollmien–Schlichting) eigenvalue, are shown in Fig. 7 for case 1 and in Fig. 8 for case 2. Therefore, the boundary layer in both cases is convectively and absolutely stable with respect to small amplitude monochromatic waves.

This result was expected for case 1. Because of the low Reynolds number of this case, the flow remains laminar. For case 2, however, both the wind-tunnel experiments and the empirical criterion indicate turbulent flow. Obviously, the relevant transition mechanism cannot be described by the linear theory. Because the critical position, where linear wave amplification first occurs, must be farther downstream, transition in our case is caused by a subcritical mechanism or a bypass mechanism.

Nonlinear Simulation Results

We performed investigations of the nonlinear stability of both cases, using the tool of numerical simulation. As in previous work on incompressible boundary-layer transition,[13,14] the temporal simulation model with periodic boundary conditions in the wall-parallel directions is used. The base profile and the Reynolds number are kept constant during the simulation. Consequently, the wall normal velocity component, as well as the boundary-layer growth, is neglected. The curved wall is approximated as a flat surface. This model has the advantage that the numerical work compared

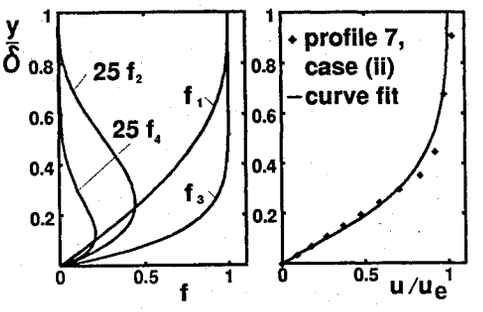

Fig. 6 Extended Pohlhausen family of interpolation functions f and example approximation.

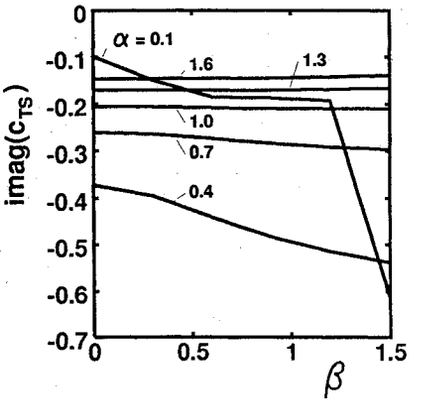

Fig. 7 Linear damping curves for profile $j = 2$ (see Table 1) of case 1.

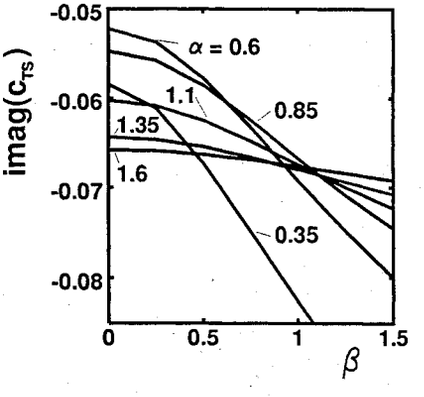

Fig. 8 Linear damping curves for profile $j = 7$ (see Table 2) of case 2.

to the spatial model is reduced. Flow structures and the transition mechanisms are known to agree qualitatively well with experimental transition investigations. The streamwise and spanwise lengths of the integration domain are arbitrarily chosen as $L_1 = L_2 = 43$, corresponding to the largest wave numbers $\alpha = 2\pi/L_1 = 0.146$ and $\beta = 2\pi/L_2 = 0.146$. The coordinate system used, x_1 (downstream), x_2 (transverse), and $x_3 = y/\delta$ (wall normal), is shown in Fig. 9.

As an initial condition a local vortex system similar to that observed by Breuer and Landahl[15] is introduced at a simulation time $t = 0$ (t is nondimensionalized with u_e and δ). The initial distribution of spanwise and normal fluxes relative to the integration domain in a plane parallel to the wall is shown in Fig. 10. The disturbance has the character of four counterrotating vortices within the boundary layer. The vortices decay near the wall and toward

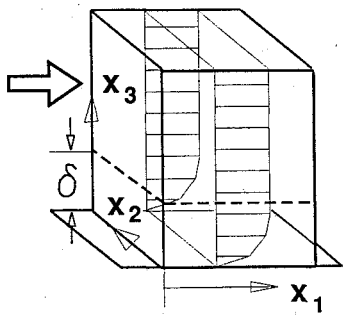

Fig. 9 Integration domain and coordinate system for the numerical simulation.

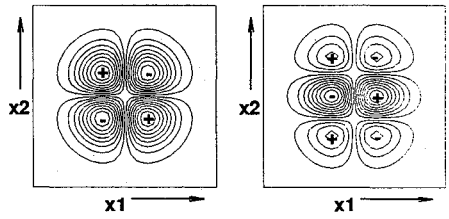

Fig. 10 Mass flux in normal direction ρu_3 (left) and in spanwise direction ρu_2 (right) at $t = 0$.

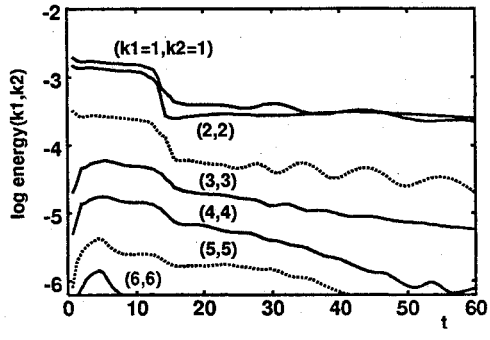

Fig. 11 Temporal development of kinetic energy contained in diagonal modes of ρu_3 for case 1.

the boundary-layer edge. The downstream velocity is zero. The amplitude of our disturbance can be controlled by a parameter A that is chosen to be 0.5 for both simulated cases corresponding to a maximum normal velocity of 3% of u_e. This disturbance can be created experimentally by a flexible wall that is moved upward and downward in a pulselike fashion.[15] Henningson et al.[16] showed that disturbances of this type lead to the development of turbulent spots (areas of developed turbulence surrounded by laminar flow) under supercritical conditions.

Numerical simulation of the disturbance development is performed by integration of the three-dimensional compressible Navier–Stokes equations in time. We use our numerical simulation method,[17–19] based on a Fourier representation of all variables in the horizontal directions x_1 and x_2 and on compact finite differences in the wall-normal direction x_3. A Crank–Nicolson scheme is employed for integration in time with the nonlinear equation system iteratively solved (three iterations). Details of the numerical scheme are given in the preceding references.

The temporal development of the disturbance amplitudes (energy content in the spatial modes $[\rho u_3](k_1, k_2)$, with the streamwise wave index k_1 and the spanwise wave index k_2) is shown in Fig. 11 for case 1 and Fig. 12 for case 2. In these figures only the modes $k_1 = k_2$ (diagonal modes) are shown, which give a good representation of the overall behavior of all modes. A maximum spatial resolution of 32×32 horizontal modes and 76 points in wall normal direction is used in case 2. This relatively high resolution of 76 points in x_3 was chosen to avoid a grid-dependent numerical instability observed in Ref. 16 when only 33 real modes (each mode approximately corresponding to one grid point of our fourth-order scheme) were used. That numerical instability, which is dominated by growing two-dimensional ($\beta = 0$) modes of high wave numbers, is not observed.

The development of the spatial structure (case 2) is depicted in Fig. 13. The initially local vortex system is stretched because of

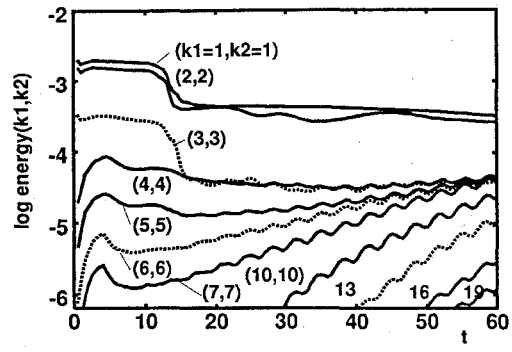

Fig. 12 Temporal development of kinetic energy contained in diagonal modes of ρu_3 for case 2.

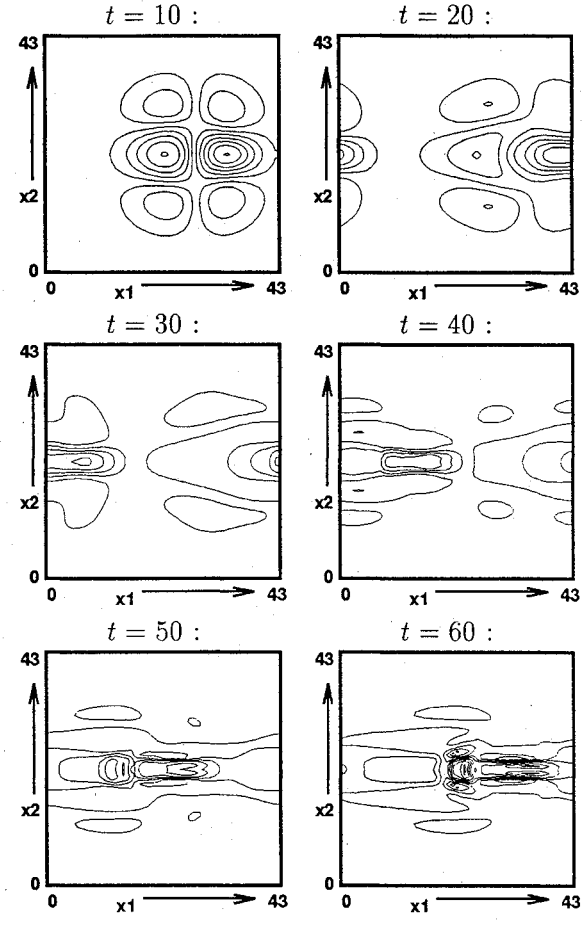

Fig. 13 Temporal development of the normal flux ρu_3 in a plane parallel to the wall.

the mean shear in the boundary layer and travels downstream (as a consequence of the periodicity of the integration domain it appears upstream when leaving the downstream end of the domain). The flow becomes locally more and more complicated.

The spatial structure of the developed disturbance at $t = 60$ is shown in Fig. 14 at various streamwise positions x_1 of the integration domain. It becomes obvious that this structure is a complex system of vortices that interact with each other and create continuously new smaller vortices. Another visualization shown in Fig. 15 has great similarity with a turbulent spot in an early stage of development. In our simulation results of case 1 it is observed that all modes are damped, but amplification occurs for case 2.

To verify that this amplification depends on the amplitude of the initial disturbance and is, therefore, a nonlinear effect, low-amplitude simulations were performed for case 2 with an initial amplitude $A = 0.005$, and completely different behavior was found (results are presented in Ref. 20 and compared with case 2). In this context note that some low-wave-number two-dimensional modes in the low-amplitude case grow slowly in an algebraic (in contrast

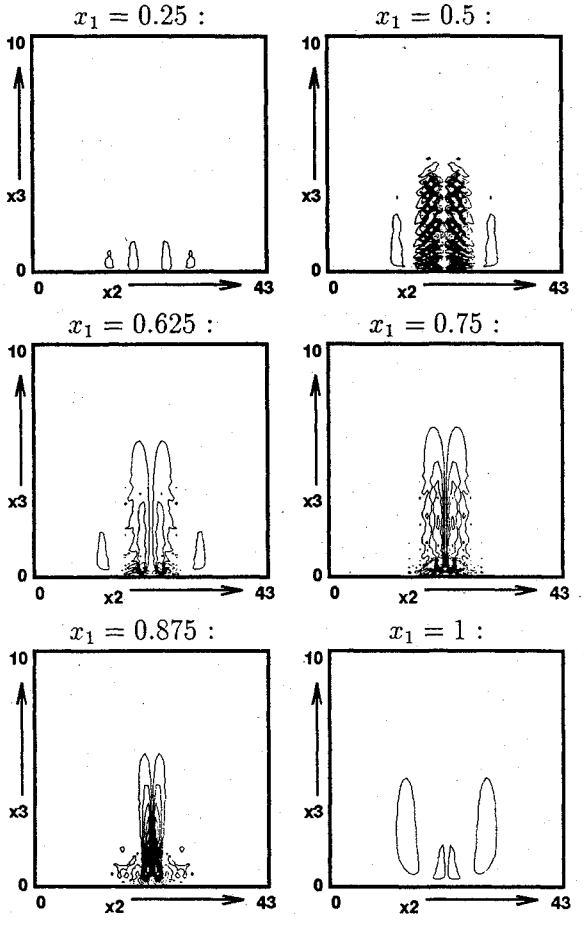

Fig. 14 Downstream vorticity in cross sections at various downstream positions, $t = 60$, case 2.

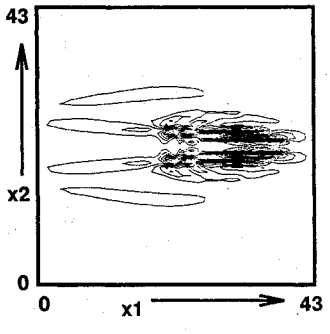

Fig. 15 Downstream vorticity in a plane parallel to the wall at $t = 60$.

to exponential) fashion. This growth, however, does not lead to transition within the simulated time interval.

Our simulation has been continued up to a state (at $t = 60$) where the highest wave number modes are approximately two orders of magnitude smaller than the long wave number modes. This means that the finite numerical resolution begins to have a visible effect on the representation of the flow in physical space and, therefore, the computation could only be continued with higher spatial resolution.

Conclusion

Our simulation results indicate that the local finite amplitude disturbance leads to the development of a turbulent spot in case 2 but does not in case 1. This behavior is consistent with the expected formation of turbulence in these cases. It may, therefore, be concluded that the relevant transition mechanism in the boundary layer of blunt bodies under re-entry conditions is the formation of turbulent spots. In contrast to the flight conditions of transonic airplanes or slender hypersonic airplanes, disturbances present in the flow are large enough to initiate spot formation. As the flow is linearly stable, the transition mechanism must be denoted with the term subcritical. It is shown schematically in Fig. 16.

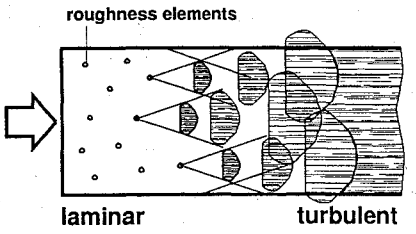

Fig. 16 Laminar turbulent transition mechanism in the boundary layer of a re-entry capsule.

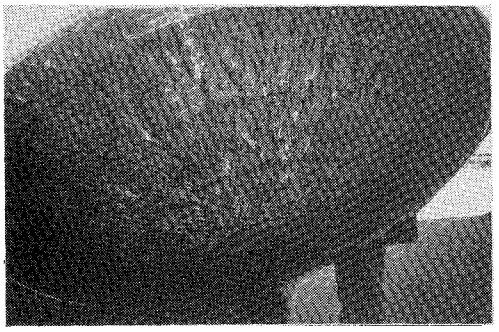

Fig. 17 Photograph of the heat shield of a Gemini capsule.

A close view on the heat shield of a Gemini capsule (Fig. 17) shows that phenomena such as turbulent wedges are present. Those wedges could be created by turbulent spots, when the disturbance source is associated with a discrete surface roughness. Those roughness elements (up to 1 cm in depth) are clearly present on any ablative heat shield.

Laminar-turbulent transition of re-entry capsules cannot be described by linear stability theory. Therefore, the e^N method, which is well established in other applications, is not relevant here. New transition prediction methods based on turbulent spot formation must be developed. Perhaps numerical simulation can make substantial contributions to these methods, because the conditions under which spot formation is possible can, in principle, be numerically predicted, as demonstrated in this work.

References

[1]Bushnell, D. M., Malik, M. R., and Harvey, W. D., "Transition Prediction in External Flows via Linear Stability Theory," *Symposium Transsonicum III*, edited by J. Zierep and H. Oertel, Springer, Berlin, 1988, pp. 225–242.

[2]Zoby, E. V., "Analysis of STS-2 Experimental Heating Rates and Transition Data," *Journal of Spacecraft and Rockets*, Vol. 20, No. 3, 1983, pp. 232–237.

[3]Widhopf, G. F., and Hall, R., "Transitional and Turbulent Heat Transfer Measurements on a Yawed Blunt Conical Nosetip," *AIAA Journal*, Vol. 10, No. 10, 1972, pp. 1318–1325.

[4]Herbert, T., and Esfahanian, V., "Stability of Hypersonic Flow over a Blunt Body," AGARD CP-514, April 1993, pp. 28-1–28-12.

[5]Reed, H. L., Stuckert, G. K., and Haynes, T. S., "Stability of Hypersonic Boundary-Layer Flows with Chemistry," AGARD CP-514, April 1993, pp. 29-1–29-13.

[6]Simen, M., and Dallmann, U., "On the Instability of Hypersonic Flow Past a Pointed Cone—Comparison of Theoretical and Experimental Results at Mach 8," AGARD CP-514, April 1993, pp. 31-1–31-13.

[7]Oertel, H., Jr., "The Aerothermodynamic Validation Reentry Experiment HYPERBA," *Orbital Transport—Technical, Meteorological, and Chemical Aspects*, Springer, Berlin, 1994, pp. 103–128.

[8]Laurien, E., Böhle, M., Holthoff, H., Wiesbaum, J., and Lieseberg, A., "Finite-Element Algorithm for Chemically Reacting Hypersonic Flows," AIAA Paper 92-0754, Jan. 1992.

[9]Löhner, R., Morgan, K., and Zienkiewicz, O. C., "An Adaptive Finite Element Procedure for Compressible High Speed Flows," *Computational Methods in Applied Mechanics and Engineering*, Vol. 51, No. 1, 1985, pp. 441–465.

[10]Wiesbaum, J., Holthoff, H., and Laurien, E., "Experiences with the Taylor–Galerkin Finite-Element Method of Hypersonic Aerothermodynamics on Supercomputers," *Flow Simulation with High-Performance Computers I*, Notes on Numerical Fluid Mechanics, Vol. 38, Vieweg, Braunschweig, Germany, 1993, pp. 379–392.

[11]Böhle, M., Holthoff, H., Laurien, E., and Wiesbaum, J., "Sensitivity Analysis of the Chemical Behavior of Reentry Flows in Nonequilibrium," AIAA Paper 94-2052, June 1994.

[12]Holthoff, H., "Numerische Simulation des Wärmeübergangs in Hyperschallströmungen," ZLR-Rept. 96-1, Technical Univ. of Braunschweig, Germany, 1996.

[13]Laurien, E., and Kleiser, L., "Numerical Simulation of Boundary-Layer Transition and Transition Control," *Journal of Fluid Mechanics*, Vol. 199, Feb. 1989, pp. 403–440.

[14]Biringen, S., and Laurien, E., "Nonlinear Structures of Transition in Wall-Bounded Flows," *Applied Numerical Mathematics*, Vol. 7, No. 1, 1991, pp. 129–150.

[15]Breuer, K. S., and Landahl, M., "The Evolution of a Localized Disturbance in a Laminar Boundary Layer. Part 2. Strong Disturbances," *Journal of Fluid Mechanics*, Vol. 220, Nov. 1990, pp. 595–621.

[16]Henningson, D. S., Lundbladh, A., and Johansson, A. V., "A Mechanism for Bypass Transition in Wall-Bounded Shear Flows," *Journal of Fluid Mechanics*, Vol. 250, May 1993, pp. 169–207.

[17]Laurien, E., Delfs, J., and Bohnsack, E., "A Spectral Method for the Numerical Simulation of Compressible Boundary-Layer Transition," *ZAMM*, Vol. 73, No. 6, 1993, pp. T 517–T 520.

[18]Delfs, J., "Numerische Simulation der transtionellen schallnahen Plattengrenzschichtströmung," ZLR-Rept. 94-05, Technical Univ. of Braunschweig, Germany, May 1994.

[19]Laurien, E., and Delfs, J., "Direct Simulation of Turbulence Phenomena in Compressible Boundary Layers," *Proceedings of the First ERCOFTAC Workshop on Direct and Large-Eddy Simulation*, edited by P. R. Voke, L. Kleiser, and J.-P. Chollet, Kluwer Academic, Dordrecht, The Netherlands, 1994, pp. 347–358.

[20]Laurien, E., "Numerical Simulation of Boundary-Layer Instabilities on Reentry Capsules," *ZAMM*, Vol. 75, SI, 1995, pp. S391–S392.

K. J. Weilmuenster
Associate Editor